Desalination and Water Treatment
www.deswater.com

doi: 10.5004/dwt.2018.21830

104 (2018) 51–61
February

Influence of surface properties of PVDF/MWNT$_{HPAE}$ nanocomposite membrane on the antibiofouling performance

Xiaoyu Zhao[a], Dongwei Lu[b,*], Meiyu Zheng[a], Yumeng Zhao[b], Jun Ma[b], Jianmin Gu[c]

[a]*Department of Chemical and Medical Engineering, Suihua University, Suihua 152061, China, emails: zhaoxy833@163.com (X. Zhao), 280363151@qq.com (M. Zheng)*
[b]*State Key Laboratory of Urban Water Resource and Environment, Harbin Institute of Technology, National Engineering Research Center of Urban Water Resources, Harbin 150090, China, emails: lvdongwei126@126.com (D. Lu), zhaoyumeng@hit.edu.cn (Y. Zhao), majun05@126.com (J. Ma)*
[c]*Hebei Key Laboratory of Applied Chemistry, School of Environmental and Chemical Engineering, Yanshan University, Qinhuangdao 066004, China, email: jianmingu79@hit.edu.cn*

Received 15 June 2017; Accepted 19 December 2017

ABSTRACT

The incorporation of carbon nanotubes into membranes has attracted a great deal of attention due to their strong antibiofouling property. Hyperbranched poly(amine-ester) functionalized multiwalled carbon nanotubes (MWNT$_{HPAE}$) were prepared to develop poly(vinylidene fluoride) (PVDF)/MWNT$_{HPAE}$ nanocomposite membranes in our previous work. The prepared nanocomposite membranes had higher water transport and less protein adsorption than PVDF membrane. In this paper, we further investigated the effects of surface properties of PVDF/MWNT$_{HPAE}$ nanocomposite membranes (hydrophilicity, surface charge and roughness) on their antimicrobial performance under no filtration condition. Antibacterial activity test indicated that no inactivation of model bacteria (*Escherichia coli* K12) was observed. The bacterial cells attached on the surface of the PVDF/MWNT$_{HPAE}$ nanocomposite membrane were less than that of the PVDF membrane. The number of attached bacterial cells decreased with the increasing concentration of MWNT$_{HPAE}$. The results demonstrated that incorporation of MWNT$_{HPAE}$ could enhance the antibiofouling performance of PVDF membrane.

Keywords: Poly(vinylidene fluoride); Multiwalled carbon nanotubes; Hydrophilicity; Hyperbranched poly(amine-ester); Antibiofouling

1. Introduction

Poly(vinylidene fluoride) (PVDF) has become one of the most popular polymeric membrane materials with regard to its outstanding properties, such as high mechanical strength, excellent chemical resistance and good thermal stability [1]. However, it suffers greatly from membrane fouling during practical application because of its hydrophobic nature. Among all types of membrane fouling, the biofouling by microorganisms is recognized as one of the most difficult treated phenomenon because microorganisms are negatively charged and relatively hydrophobic [2]. These microorganisms tend to attach to the hydrophobic surface, which could increase the surface roughness of the substrate [3]. In addition, it was reported that microorganisms were prone to grow on a rough surface. Thus, biofouling can damage membrane surfaces, shorten membrane life and ultimately lead to the cost increase for membrane replacement [4]. It is of greatly scientific interest and technological significance to develop a facile route for the preparation of the PVDF membrane materials with the antibiofouling performance in water treatment field.

Membrane surface characteristics (such as hydrophilicity/hydrophobicity, surface roughness and surface charge) can influence microorganism attachment [5]. Membrane surface modification is an efficient technique to reduce membrane biofouling [6]. For example, membranes have been designed

* Corresponding author.

to prevent cell from attachment by increasing the hydrophilicity through coating hydrophilic polymers [7], blending with hydrophilic polymers [8] and grafting hydrophilic monomers on membrane surface [9]. In addition to the classical nanoparticles such as Ag, Al_2O_3, ZrO_2, graphene oxide, etc. [10–13], carbon nanotubes have attracted considerable attention owing to the antibacterial activity [14]. The micrometer-size deposit layers of either single-walled carbon nanotubes or multiwalled carbon nanotubes (MWNTs) on a microporous membrane have been developed, and their filtration performance in terms of the removal and inactivation of viruses and bacteria has been investigated [15,16]. In our previous work, MWNTs were functionalized with hyperbranched poly(amine-ester), and then used as additive to prepare PVDF nanocomposite membranes via phase inversion method [17]. Functionalization of MWNTs with hyperbranched poly(amine-ester) contributed to the dissolution of MWNTs in dimethylfomamide (DMF), reduced their hydrophobicity and decreased their aggregation and size polydispersity. On the other hand, MWNTs grafted with hyperbranched poly(amine-ester) formed hydrogen bonds with surrounding water molecules to reconstruct a hydrated layer on membrane surface, and thus inducing steric repulsion. Accordingly, the proteins were prevented from attaching to membranes [17].

On the base of our previous work, we evaluated the influences of primary physicochemical surface properties of the PVDF/$MWNT_{HPAE}$ nanocomposite membranes on the biofouling under no filtration condition. Various techniques such as atomic force microscopy (AFM), streaming potential and contact angle goniometry were applied to characterize the surface properties of nanocomposite membranes. Difference in bacterial counts on the membranes before and after modification was compared to evaluate their biofouling resistance. The results can provide a useful enlightenment for the development of novel nanocomposite biofouling-resistant membranes.

2. Materials and methods

2.1. Materials and chemicals

The MWNTs were obtained from Chengdu Organic Chemicals Co., Ltd. (Chengdu). The average diameter of the nanotubes was 10–20 nm with 30 μm in length and the pure MWNTs content was more than 95 wt%. PVDF was purchased from Shanghai 3F New Materials Co., Ltd. (Shanghai) (FR904, M_w = 475,637). DMF (Sinopharm Chemical Reagent Co., Ltd., (Shanghai) >99%, Analytical Reagent) and distilled water were used as solvent and nonsolvent for the casting solution, respectively. Trimethanol propane was purchased from TCI Shanghai (Shanghai) (98%). Diethanolamine, *p*-toluene sulfonic acid, methanol, methyl acrylate, acetone, ethanol, HNO_3 (67%) and H_2SO_4 (98%) were purchased from Tianjin Guangfu Fine Chemical Research Institute (Tianjin). *Escherichia coli* (*E. coli*) K12 was purchased from Chinese Academy of Science (Beijing). SYBR Green I and propidium iodide (PI) were purchased from Invitrogen Company (Changsha). All the materials were used as-received without further purification.

2.2. Preparation of nanocomposite biofouling-resistant membranes

In a typical synthesis, the PVDF ultrafiltration membranes are prepared by the immersion precipitation method [17]. Briefly, different amounts (0 wt%–2 wt% of PVDF dosage, respectively) of $MWNT_{HPAE}$ were poured into a certain amount (85 wt%, respectively) of DMF, ultrasonicated for 30 min to ensure complete dispersion. After dispersing $MWNT_{HPAE}$ in DMF, PVDF (15 wt% in casting solutions) was dissolved in the dope solution by continuous stirring and heating at 60°C for 10 h to ensure a complete dissolution. After fully degassing, the casting dope was cast at a thickness of 200 μm on a clean glass plate. The membrane was immediately immersed in coagulation bath (distilled water). After peeling off from the glass plates, the membrane was rinsed in distilled water in the refrigerator prior to use.

2.3. Membrane characterization

2.3.1. Surface hydrophilicity

The hydrophilicity of membrane surfaces was evaluated by contact angle measurement [18–20]. The static contact angles of the membrane surface were measured by the sessile drop method with contact angle goniometer (QSPJ-360 Contact Angle Meter, Jinshengxin Co., Beijing, China).

2.3.2. Surface roughness

Surface morphology of clean membranes was evaluated using (AFM (Digital Instruments, Veeco Metrology Group, USA) in tapping mode [21]. The captured images were analyzed by Nanoscope III AFM image processing software version 5.12. AFM analyses were performed in dry conditions. The virgin membrane roughness was determined from images of 5 μm × 5 μm areas.

2.3.3. Streaming potential

The zeta potential of coated and uncoated membranes was determined using an Anton Paar Surpass Electrokinetic Analyzer (Anton Paar USA, Ashland, VA) based on the streaming potential measurements. The results were obtained using the clamping cell apparatus and the 1 mM KCl as the background solution. The values reported are used only 1 mM KCl as electrolyte, which has a pH of 4.5 ± 0.3. Four measurements were recorded and the average was reported [22].

2.3.4. Scanning electron microscopy

All clean and fouled membranes samples were placed on the aluminum mount and sputter coated with gold for 10 min prior to imaging. The morphology of the membranes was observed by field emission scanning electron microscopy with a Philip XL-30-ESEM-FEG microscope made in Holland, operated at 20 kV [23].

2.4. Antibacterial experiments

2.4.1. Preparation of the bacterial cells

E. coli K12 was grown in Luria Bertani broth medium at 37°C and harvested in the exponential growth phase (around 16 h). After collected, cells were washed twice and then resuspended in an isotonic solution (0.8% NaCl, pH 5.7) [24].

2.4.2. Antibacterial activity property tests

To evaluate the antibacterial activity of the nanocomposite membrane, cells (10^7 cells/mL) in an isotonic solution (0.8% NaCl, pH = 5.7) were added on the membrane (30 mm × 30 mm), which was placed in Petri dishes. The active side of the membrane was in contact with the cell suspension for 1 h at 37°C. After incubation, membranes were rinsed with phosphate buffer saline and then sonicated by sonication device for 7 min to detach deposited bacteria from the membrane surface. Cell amount and viability loss were performed by flow cytometry. Cell amount was quantified by SYBR Green I and viability loss was evaluated with SYBR Green I plus PI. The percentage of dead cells (or loss of viability) was determined from the ratio of the number of cells stained with PI divided by the number of cells stained with SYBR Green I plus PI. All samples were performed in triplicate and inactivation rates were determined by comparing the integrity cell density of the modified membranes in comparison with the control membrane [24–26].

2.4.3. Bacterial quantification and viability assessment by flow cytometry

Microbial amount and viability for each sample were determined by counting the number of microbes by flow cytometry. Determination of total microbial amount with flow cytometry was performed as previously described [25]. Briefly, 5 μL of SYBR Green I (1:100 dilutions in DMSO) was added to 0.5 mL of sample and then incubated in the dark for 10 min at 30°C. Flow cytometry was performed using an Accuri C6 instrument, equipped with a blue 25 mW solid state laser emitting light at a fixed wavelength of 488 nm. FL1 was collected at 520 ± 10 nm, FL3 at 630 nm and sideward scatter at 488 nm. The Accuri C6 instrument has a quantification limit of 1,000 cells/mL.

Viability assessment using PI (30 mM) was measured by flow cytometry following the method described previously [26]. Briefly, 5 μL of SYBR Green I (1:100 dilution in DMSO) plus PI (0.3 mM) was added to 0.5 mL of sample and then incubated in the dark for 10 min at 30°C. The results were recorded with a dot-plot diagram. PI can go through compromised membrane and red fluorescence would be detected in those cells.

2.4.4. Static bacterial adhesion tests

To evaluate the antibacterial adhesion property of the nanocomposite membrane, bacterial amount was measured by flow cytometry as described. In addition, the number of cells was also determined by scanning electron microscopy (SEM) [27]. After removal from the filtered water, membranes were gently rinsed with phosphate buffered saline to remove any unbound organic matter. Three replicate 3 cm × 3 cm samples per membrane were fixed with 2.5% glutaraldehyde and post-fixed in 1% osmium tetroxide. Subsequently, the samples were dehydrated in a graded series of ethanol (30%, 50%, 70%, 80%, 90%, 95% and 100% v/v). The samples were then dried at room temperature before preparation for SEM [28].

3. Results and discussion

3.1. Membrane properties

3.1.1. Morphology of the membranes

Figs. S1 and S2 show the cross-section and surface morphologies of membranes with different blend compositions. It can be seen that all membranes showed a typical asymmetric membrane structure (Figs. S1(a)–(e)). The pore size increased with $MWNT_{HPAE}$ contents up to 1.5 wt% and then decreased (Fig. S2).

3.1.2. Hydrophilicity analysis

A correlation between membrane surface hydrophilicity and membrane fouling resistance has been addressed in Wavhal and Fisher [29] and Ju et al. [30]. Higher fouling resistance is expected for more hydrophilic surfaces. To evaluate the hydrophilicity of $MWNT_{HPAE}$, the water contact angle of the membranes was measured. As shown in Table 1, the PVDF membrane possessed the highest water contact angle of 85° ± 1.3°, while the water contact angles of the PVDF/$MWNT_{HPAE}$ nanocomposite membranes decreased from 80° ± 0.8° to 73° ± 1.1° with the increasing ratio of $MWNT_{HPAE}$ from 0.5% to 2%. These results suggest that the hydrophilicity of membrane surface increased after the incorporation of $MWNT_{HPAE}$. The $MWNT_{HPAE}$ with –OH functional groups was introduced on the surface of the PVDF/$MWNT_{HPAE}$ nanocomposite membrane (Fig. S3), and changed the chemical properties of membrane surface.

3.1.3. Roughness analysis

AFM is an effective technique for the analysis of the roughness parameters and can be used to observe the heterogeneous topography among the nanocomposite

Table 1
Surface parameters, water contact angle and zeta potential of the membranes

Membrane	Zeta potential (eV)	Water contact angle (°)	Surface parameters		
			Z	R_q	R_a
PVDF	–27.42	85 ± 1.3	362.90	55.311	43.740
PVDF/$MWNT_{HPAE}$-0.5	–19.21	80 ± 0.8	295.00	40.532	32.071
PVDF/$MWNT_{HPAE}$-1	–16.68	78 ± 0.6	319.09	44.626	35.855
PVDF/$MWNT_{HPAE}$-1.5	–20.69	75 ± 1.2	324.95	48.923	40.379
PVDF/$MWNT_{HPAE}$-2	–18.71	73 ± 1.1	524.93	52.132	42.526

membranes [21]. Fig. 1 shows the three-dimensional AFM surface images of the PVDF and PVDF/MWNT$_{HPAE}$ nanocomposite membranes. Differences in the membrane surface morphology can be expressed in terms of various roughness parameters such as average roughness (R_a) and root mean square of Z data roughness (R_q) [20]. Roughness parameters could be obtained through the AFM analysis software. The roughness measurements obtained with tapping mode AFM were given in Table 1. Analytically, the examined samples of PVDF, PVDF/MWNT$_{HPAE}$-0.5, PVDF/MWNT$_{HPAE}$-1, PVDF/MWNT$_{HPAE}$-1.5 and PVDF/MWNT$_{HPAE}$-2 were given R_a values of 39.778, 40.654, 42.584, 46.439 and 50.993 nm on average, respectively. The R_q for the PVDF was found to be 49.609 nm, while that for the PVDF/MWNT$_{HPAE}$-0.5, PVDF/MWNT$_{HPAE}$-1, PVDF/MWNT$_{HPAE}$-1.5 and PVDF/MWNT$_{HPAE}$-2 nanocomposite membranes were 51.295, 52.921, 59.074 and 66.308 nm, respectively. These results indicated that the surface roughness increased with the increasing content of MWNT$_{HPAE}$.

3.1.4. Zeta potential analysis

The zeta potential values for PVDF and PVDF/MWNT$_{HPAE}$ nanocomposite membranes are also reported in Table 1. As shown in Table 1, the PVDF membrane had the greatest negative surface charge of –27.42 mV, wherever the negative surface charges (zeta potentials) of PVDF/MWNT$_{HPAE}$ nanocomposite membranes were slightly less than that of PVDF membranes. This behavior was expected, as HPAE possesses the quaternary ammonium ion, which is positively charged at pH = 4.5 [22]. In addition, the zeta potential values for PVDF/MWNT$_{HPAE}$ nanocomposite membranes were close to each other except PVDF/MWNT$_{HPAE}$-1 nanocomposite membrane which had the smallest negative surface charge at –16.68 mV.

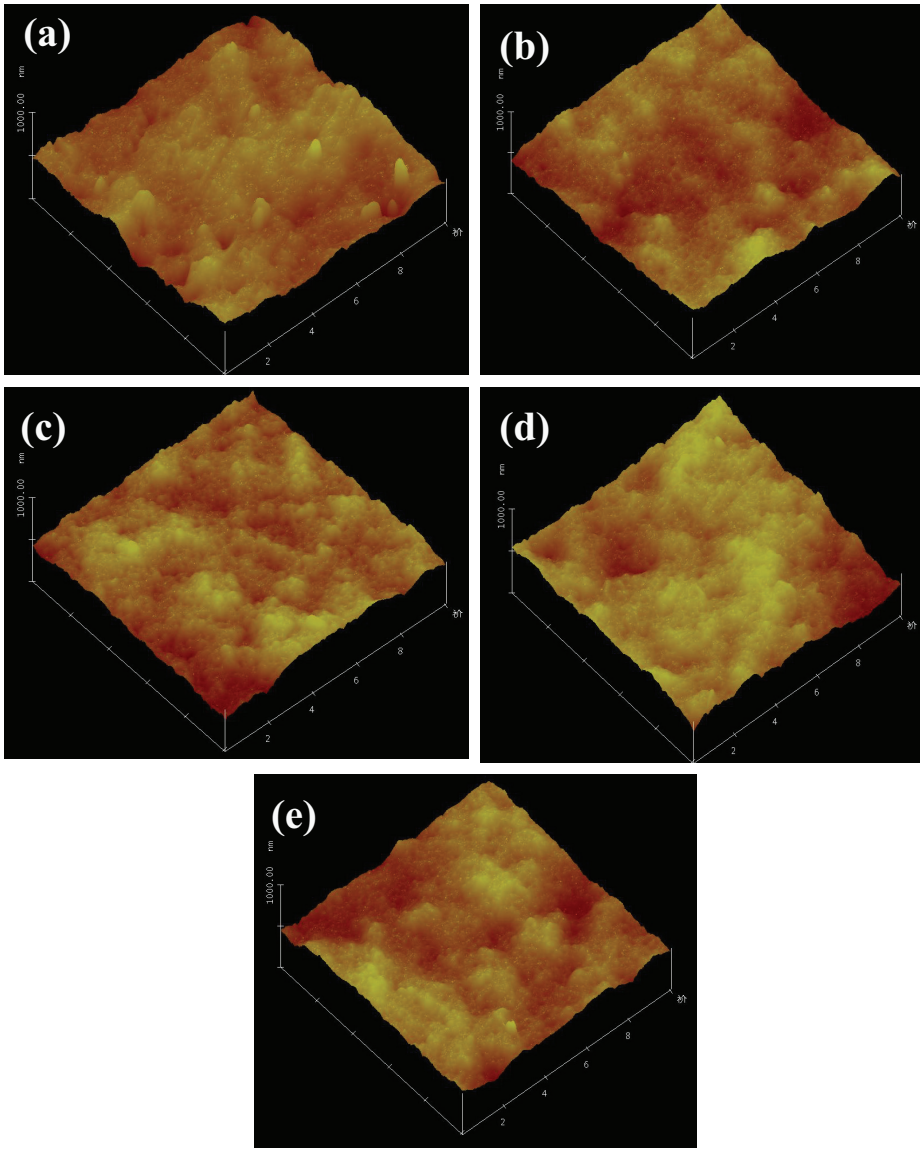

Fig. 1. AFM stereoscopic images of the membranes: (a) PVDF, (b) PVDF/MWNT$_{HPAE}$-0.5, (c) PVDF/MWNT$_{HPAE}$-1, (d) PVDF/MWNT$_{HPAE}$-1.5 and (e) PVDF/MWNT$_{HPAE}$-2.

3.2. Antibiofouling performance

3.2.1. Antibacterial activity study

To assess inactivation of bacteria by PVDF/MWNT$_{HPAE}$ nanocomposite membrane, we compared the number of viable cells present on a control PVDF membrane with that of viable cells present on the PVDF/MWNT$_{HPAE}$ nanocomposite membrane. Fig. 2 shows that no *E. coli* inactivation after incubation with PVDF and PVDF/MWNT$_{HPAE}$ nanocomposite membranes. It may be attributed that the contact probability with cells is too small to display the cytotoxicity, although MWNT$_{HPAE}$ was distributed on the surface of PVDF membrane by X-ray photoelectron spectroscopy (XPS) [15–17].

3.2.2. Antibacterial adhesion studies

Membrane materials have an extremely high biofouling potential in aquatic environments [2]. Biofouling was expressed as the variations of total adhered cells [3]. The degree (number of cells per cm^2) of bacterial adhesion (live and dead) on each membrane is shown in Fig. 2. As shown in Fig. 2, the degree of bacterial adhesion on the PVDF membrane was higher than that on the PVDF/MWNT$_{HPAE}$ nanocomposite membrane. The number of attached bacterial cells decreased with the increasing concentration of MWNT$_{HPAE}$. These results suggested that nanocomposite membrane mitigated the biofouling.

Besides the flow cytometer, the variation of bacterial population is clearly seen with SEM in Fig. 3. It shows typical SEM images of prepared membranes after exposure to the cell suspension for 1 h at 37°C to compare the number of the bacteria attached on the different membranes. As shown in Fig. 3(a), significant adhesion of bacterial cells was observed on the PVDF surface. In contrast, fewer bacteria can be found on the PVDF/MWNT$_{HPAE}$ nanocomposite membrane surface after exposure to the cell suspension for 1 h at 37°C (Figs. 3(b)–3(e)).

3.3. The relationship between membrane properties and antifouling performance

Fig. 4 shows the degree (number of cells per cm^2) of bacterial adhesion on each membrane with increasing MWNT$_{HPAE}$ content in the antibacterial adhesion study (a), and roughness, zeta potential and contact angle (b–d). As shown in Fig. 4(a), the number of cells attached on the membranes decreased as the MWNT$_{HPAE}$ content increased, and all the PVDF/MWNT$_{HPAE}$ nanocomposite membranes had less bacterial adhesion than sole PVDF. Fig. 4(b) shows hydrophilicity/hydrophobicity vs. the degree of bacterial adhesion. Clearly, it was shown that the degree of bacterial adhesion decreased with the increase of hydrophilicity. Fig. 4(c) exhibits surface roughness vs. the degree of bacterial adhesion. The degree of bacterial adhesion showed

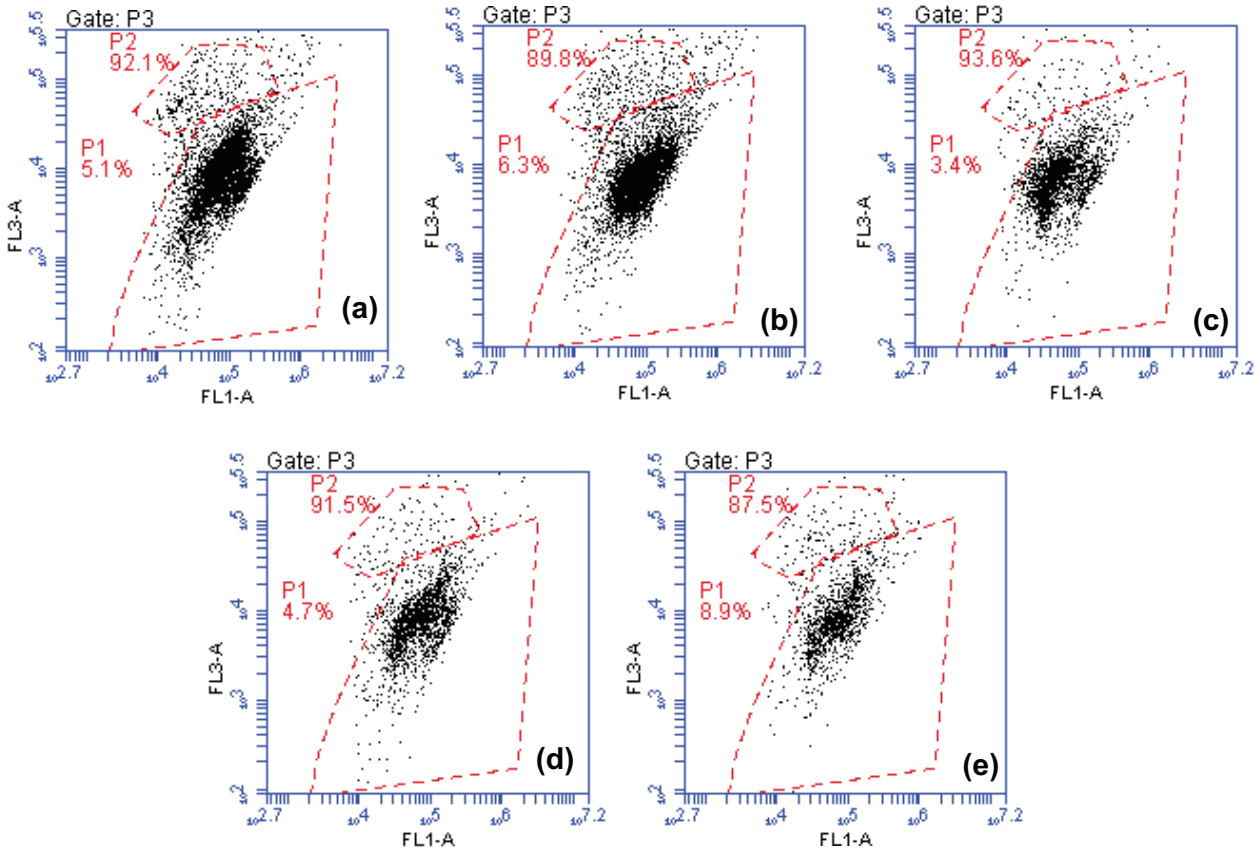

Fig. 2. The effect of MWNT$_{HPAE}$ content for the *E. coli* of membrane surface: (a) PVDF, (b) PVDF/MWNT$_{HPAE}$-0.5, (c) PVDF/MWNT$_{HPAE}$-1, (d) PVDF/MWNT$_{HPAE}$-1.5 and (e) PVDF/MWNT$_{HPAE}$-2.

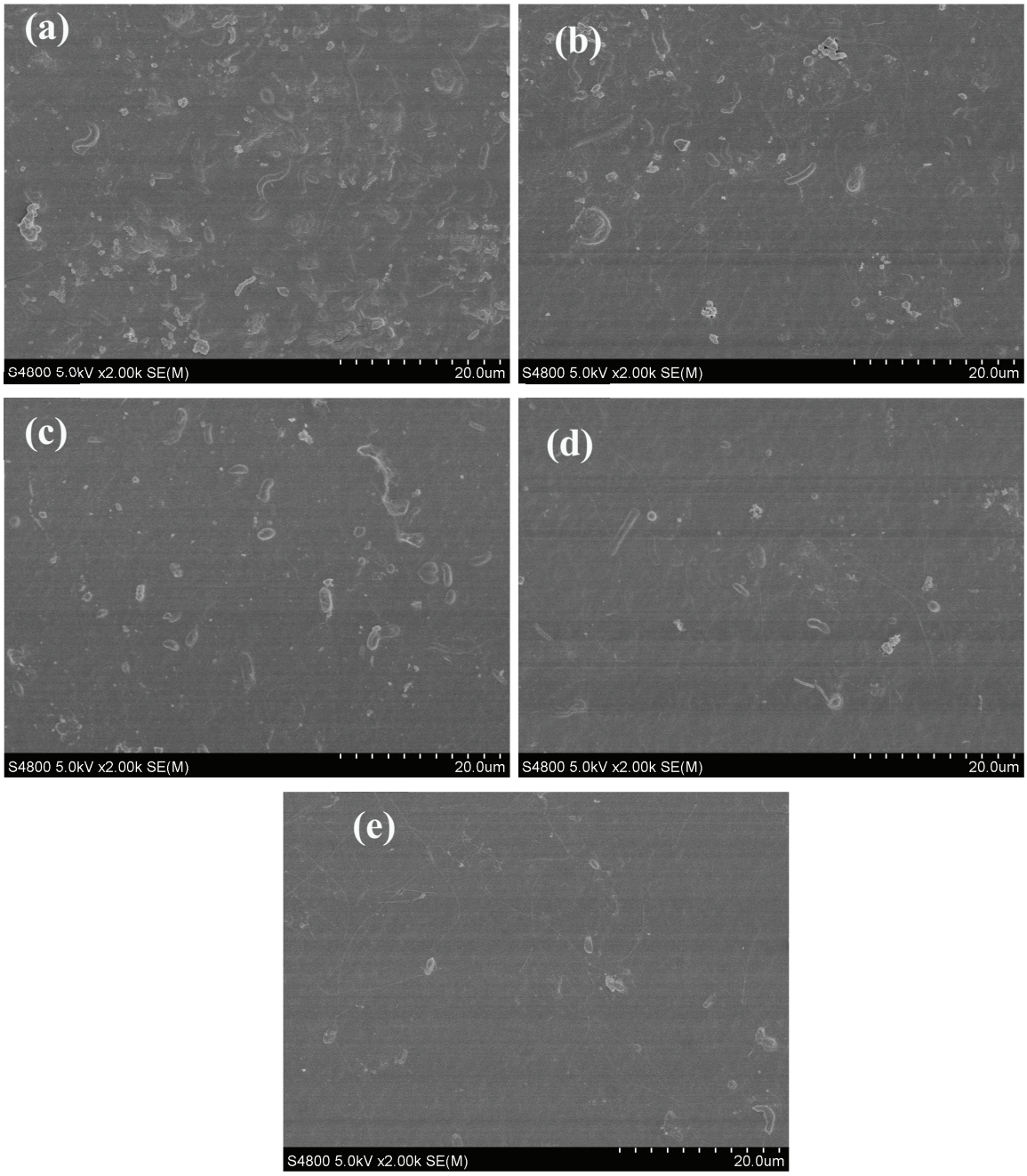

Fig. 3. Surface morphology of the membranes after exposure to the cell suspension: (a) PVDF, (b) PVDF/MWNT$_{HPAE}$-0.5, (c) PVDF/MWNT$_{HPAE}$-1, (d) PVDF/MWNT$_{HPAE}$-1.5 and (e) PVDF/MWNT$_{HPAE}$-2.

a weakly negative correlation to the surface roughness of membranes except PVDF. For instance, PVDF/MWNT$_{HPAE}$-2 nanocomposite membrane had the greatest R_a value with the least number of bacterial cells, and PVDF/MWNT$_{HPAE}$-0.5 had the smallest R_a value with the most number of attached cells. Fig. 4(d) shows the relationship between the surface charges and the degree of bacterial adhesion. As shown in Fig. 4(d), although zeta potential values for PVDF/MWNT$_{HPAE}$-0.5 nanocomposite membrane and PVDF/MWNT$_{HPAE}$-2 nanocomposite membrane were close to each other (Table 1), the attached cell number of PVDF/MWNT$_{HPAE}$-0.5 nanocomposite membrane was almost three times bigger than that of PVDF/MWNT$_{HPAE}$-2 nanocomposite membrane. This phenomenon can be attributed to the different hydrophilicity and surface roughness among PVDF/MWNTHPAE nanocomposite membranes with different dosages of MWNT$_{HPAE}$.

According to the above results, high hydrophilicity would lead low bacterial adhesion while high roughness may lead high bacterial adhesion. PVDF/MWNT$_{HPAE}$-2

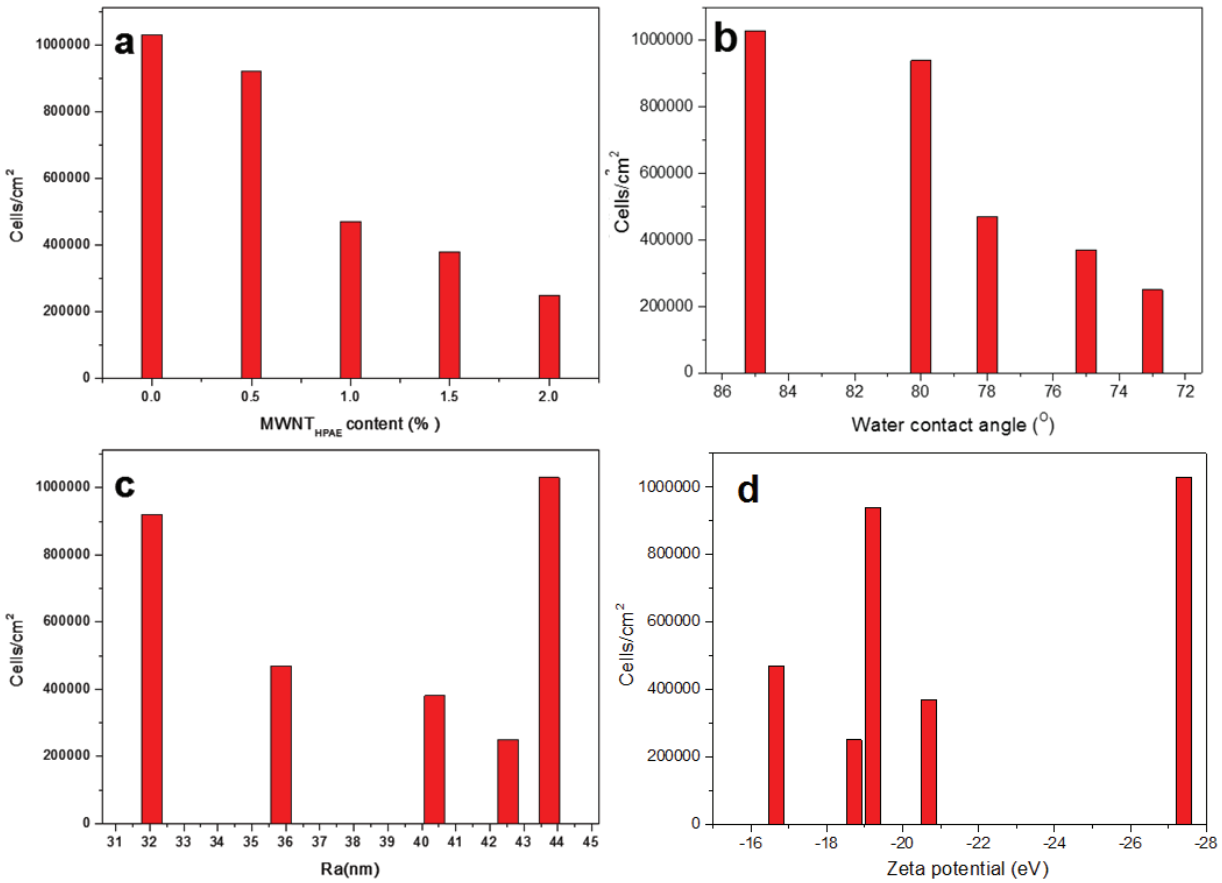

Fig. 4. The effect of surface characteristic for the bacterium adhesion: (a) MWNT$_{HPAE}$ content, (b) water contact angle, (c) surface roughness and (d) zeta potential.

nanocomposite membrane had less bacterial adhesion than PVDF/MWNT$_{HPAE}$-0.5 in Fig. 4(a), and its surface was more hydrophilic and more rough as shown in Figs. 4(b)–(d). This result demonstrated that hydrophilicity/hydrophobicity showed more influence on the bacterial adhesion. It agrees with the observations of Pasmore et al. [3], who found that microscale roughness had less effect than hydrophilicity for fouling by *Pseudomonas aeruginosa*.

4. Conclusions

In conclusion, various techniques were applied to evaluate the effect of MWNT$_{HPAE}$ on the surface properties of PVDF membrane. The results showed that PVDF/MWNT$_{HPAE}$ nanocomposite membranes exhibited relatively higher hydrophilicity and lower roughness compared with PVDF membranes. No *E. coli* inactivation was observed after incubation with PVDF and PVDF/MWNT$_{HPAE}$ nanocomposite membranes. The bacterial cells attachment on the PVDF/MWNT$_{HPAE}$ nanocomposite membrane surface was less than that of the PVDF membrane. The blending of MWNT$_{HPAE}$ can improve the antibiofouling ability of PVDF membranes. The biofouling performance of the PVDF/MWNT$_{HPAE}$ nanocomposite membrane under the condition of cross-flow filtration will be further investigated in the future work.

Acknowledgments

This work was supported by the Doctor Research Foundation of Suihua University (project's number: SD13002), National Natural Science Foundation of China (No. 21403189) and China Postdoctoral Science Foundation (No. 2014M551047) and Postdoctoral Science Foundation of Heilongjiang Province of China.

References

[1] F. Liu, N.A. Hashim, Y. Liu, M.R.M. Abed, K. Li, Progress in the production and modification of PVDF membranes, J. Membr. Sci., 375 (2011) 1–27.
[2] J. Mansouri, S. Harrisson, V. Chen, Strategies for controlling biofouling in membrane filtration systems: challenges and opportunities, J. Mater. Chem., 20 (2010) 4567–4586.
[3] M. Pasmore, P. Todd, S. Smith, D. Baker, J. Silverstein, D. Coons, C.N. Bowman, Effects of ultrafiltration membrane surface properties on *Pseudomonas aeruginosa* biofilm initiation for the purpose of reducing biofouling, J. Membr. Sci., 194 (2001) 15–32.
[4] C. Sun, L. Fiksdal, A. Hanssen-Bauer, M.B. Rye, T. Leiknes, Characterization of membrane biofouling at different operating conditions (flux) in drinking water treatment using confocal laser scanning microscopy (CLSM) and image analysis, J. Membr. Sci., 382 (2011) 194–201.
[5] E. Lee, H.K. Shon, J. Cho, Biofouling characteristics using flow field-flow fractionation: effect of bacteria and membrane properties, Bioresour. Technol., 101 (2010) 1487–1493.

[6] J. Yin, B.L. Deng, Polymer-matrix nanocomposite membranes for water treatment, J. Membr. Sci., 479 (2015) 256–275.
[7] S. Boributh, A. Chanachai, R. Jiraratananon, Modification of PVDF membrane by chitosan solution for reducing protein fouling, J. Membr. Sci., 342 (2009) 97–104.
[8] Z. Yuan, X.D. Li, Porous PVDF/TPU blends asymmetric hollow fiber membranes prepared with the use of hydrophilic additive PVP (K30), Desalination, 223 (2008) 438–447.
[9] M. Zhang, Q.T. Nguyen, Z. Ping, Hydrophilic modification of poly (vinylidene fluoride) microporous membrane, J. Membr. Sci., 327 (2009) 78–86.
[10] S.M. Meagan, Y. Wang, K.C. Okemgbo, C.O. Osuji, E.P. Giannelis, M. Elimelech, Antifouling ultrafiltration membranes via post-fabrication grafting of biocidal nanomaterials, ACS Appl. Mater. Interfaces, 3 (2011) 2861–2868.
[11] T.H. Bae, T.M. Tak, Effect of TiO_2 nanoparticles on fouling mitigation of ultrafiltration membranes for activated sludge filtration, J. Membr. Sci., 249 (2005) 1–8.
[12] L.Y. Yu, Z.L. Xu, H.M. Shen, H. Yang, Preparation and characterization of PVDF/SiO_2 composite hollow fiber UF membrane by sol–gel method, J. Membr. Sci., 337 (2009) 257–265.
[13] S. Zinadini, A.A. Zinatizadeh, M. Rahimi, V. Vatanpour, H. Zangeneh, Preparation of a novel antifouling mixed matrix PES membrane by embedding graphene oxide nanoplates, J. Membr. Sci., 453 (2014) 292–301.
[14] V.K.K. Upadhyayula, V. Gadhamshetty, Appreciating the role of carbon nanotube composites in preventing biofouling and promoting biofilms on material surfaces in environmental engineering: a review, Biotechnol. Adv., 28 (2010) 802–816.
[15] S. Kang, M. Pinault, L.D. Pfefferle, M. Elimelech, Single walled carbon nanotubes exhibit strong antimicrobial activity, Langmuir, 23 (2007) 8670–8673.
[16] S. Kang, S.M. Mauter, M. Elimelech, Physiochemical determinants of multiwalled carbon nanotube bacterial cytotoxicity, Environ. Sci. Technol., 42 (2008) 7528–7534.
[17] X.Y. Zhao, J. Ma, Z.H. Wang, G. Wen, J. Jiang, F.M. Shi, L.X. Sheng, Hyperbranched-polymer functionalized multi-walled carbon nanotubes for poly (vinylidene fluoride) membranes: from dispersion to blended fouling-control membrane, Desalination, 303 (2012) 29–38.
[18] W. Zhang, M. Wahlgren, B. Sivik, Membrane characterization by the contact-angle technique. 2. Characterization of UF-membranes and comparison between the captive bubble and sessile drop as methods to obtain water contact angles, Desalination, 72 (1989) 263–273.
[19] V. Gekas, K.M. Persson, M. Wahlgren, B. Sivik, Contact angles of ultrafiltration membranes and their possible correlation to membrane performance, J. Membr. Sci., 72 (1992) 293–302.
[20] Y.Q. Wang, T. Wang, Y.L. Su, F.B. Peng, H. Wu, Z.Y. Jiang, Protein adsorption-resistance and permeation property of polyethersulfone and soybean phosphatidylcholine blend ultrafiltration membranes, J. Membr. Sci., 270 (2006) 108–114.
[21] X.C. Cao, J. Ma, X. Shi, Z.J. Ren, Effect of TiO_2 nanoparticle size on the performance of PVDF membrane, Appl. Surf. Sci., 253 (2006) 2003–2010.
[22] J.M. Peng, Y.L. Su, Q. Shi, W.J. Chen, Z.Y. Jiang, Protein fouling resistant membrane prepared by amphiphilic pegylated polyethersulfone, Bioresour. Technol., 102 (2011) 2289–2295.
[23] Q.Z. Zheng, P. Wang, Y.N. Yang, D.J. Cui, The relationship between porosity and kinetics parameter membrane formation in PSF ultrafiltration membrane, J. Membr. Sci., 286 (2006) 7–11.
[24] J.D. Schiffman, M. Elimelech, Antibacterial activity of electrospun polymer mats with incorporated narrow diameter single-walled carbon nanotubes, ACS Appl. Mater. Interfaces, 3 (2011) 462–468.
[25] F. Hammes, M. Berney, Y. Wang, M. Vital, O. Köster, T. Egli, Flow-cytometric total bacterial cell counts as a descriptive microbiological parameter for drinking water treatment processes, Water Res., 42 (2008) 269–277.
[26] M. Berney, M. Vital, I. Hülshoff, H.U. Weilenmann, T. Egli, F. Hammes, Rapid, cultivation-independent assessment of microbial viability in drinking water, Water Res., 42 (2008) 4010–4018.
[27] S. Kang, M. Herzberg, D.F. Rodrigues, M. Elimelech, Antibacterial effects of carbon nanotubes: size does matter! Langmuir, 24 (2008) 6409–6413.
[28] Y. Bai, S. Parka II, S.J. Lee, P.S. Wen, T.S. Bae, M.H. Lee, Effect of AOT-assisted multi-walled carbon nanotubes on antibacterial activity, Colloids Surf., B, 89 (2012) 101–107.
[29] D.S. Wavhal, E.R. Fisher, Hydrophilic modification of polyethersulfone membranes by low temperature plasma-induced graft polymerization, J. Membr. Sci., 209 (2002) 255–269.
[30] H. Ju, B.D. McCloskey, A.C. Sagle, V.A. Kusuma, B.D. Freeman, Preparation and characterization of crosslinked poly (ethylene glycol) diacrylate hydrogels as fouling resistant membrane coating materials, J. Membr. Sci., 330 (2009) 180–188.

Supporting information

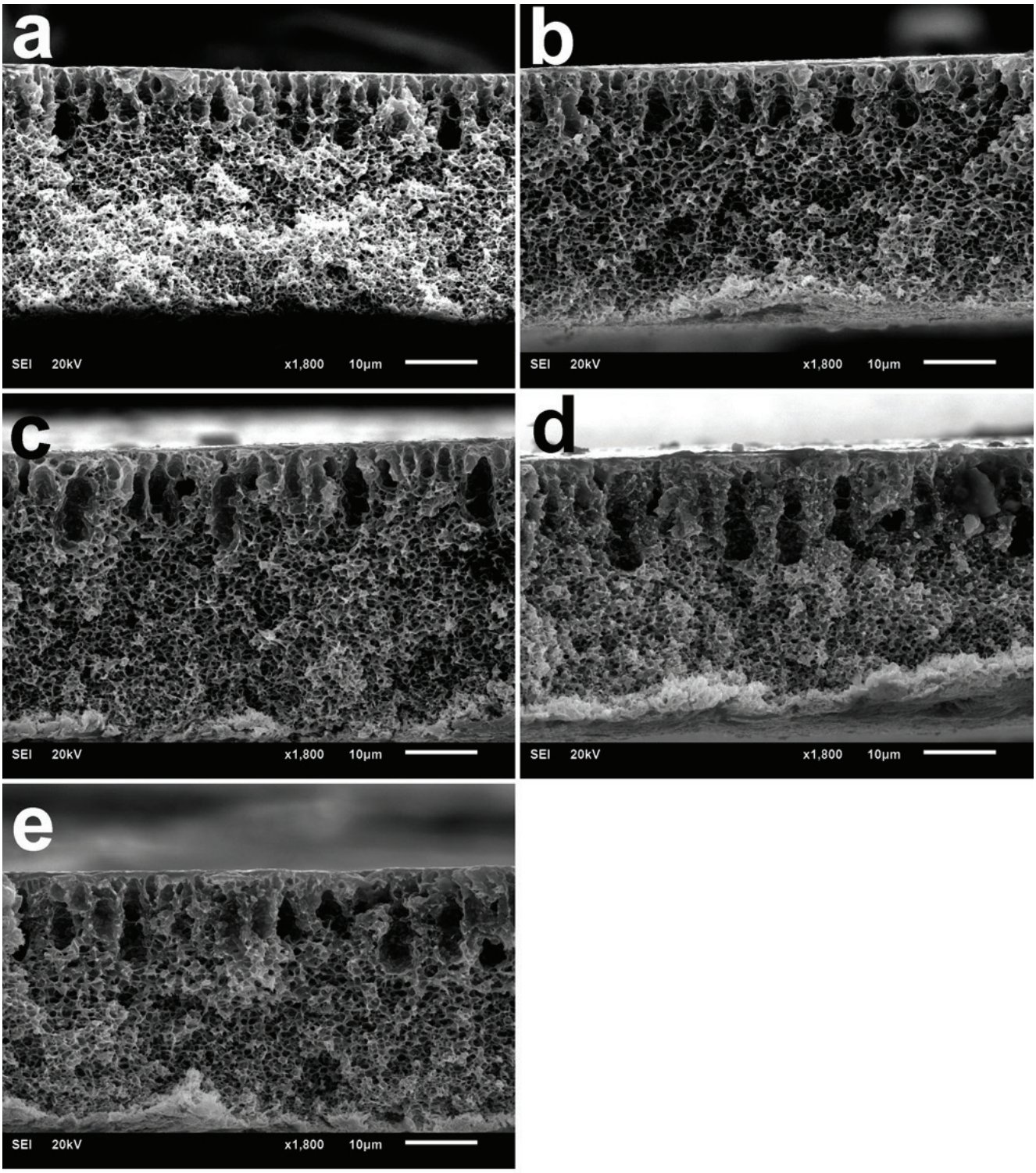

Fig. S1. Cross-section morphology of the membranes: (a) PVDF, (b) PVDF/MWNT$_{HPAE}$-0.5, (c) PVDF/MWNT$_{HPAE}$-1, (d) PVDF/MWNT$_{HPAE}$-1.5 and (e) PVDF/MWNT$_{HPAE}$-2.

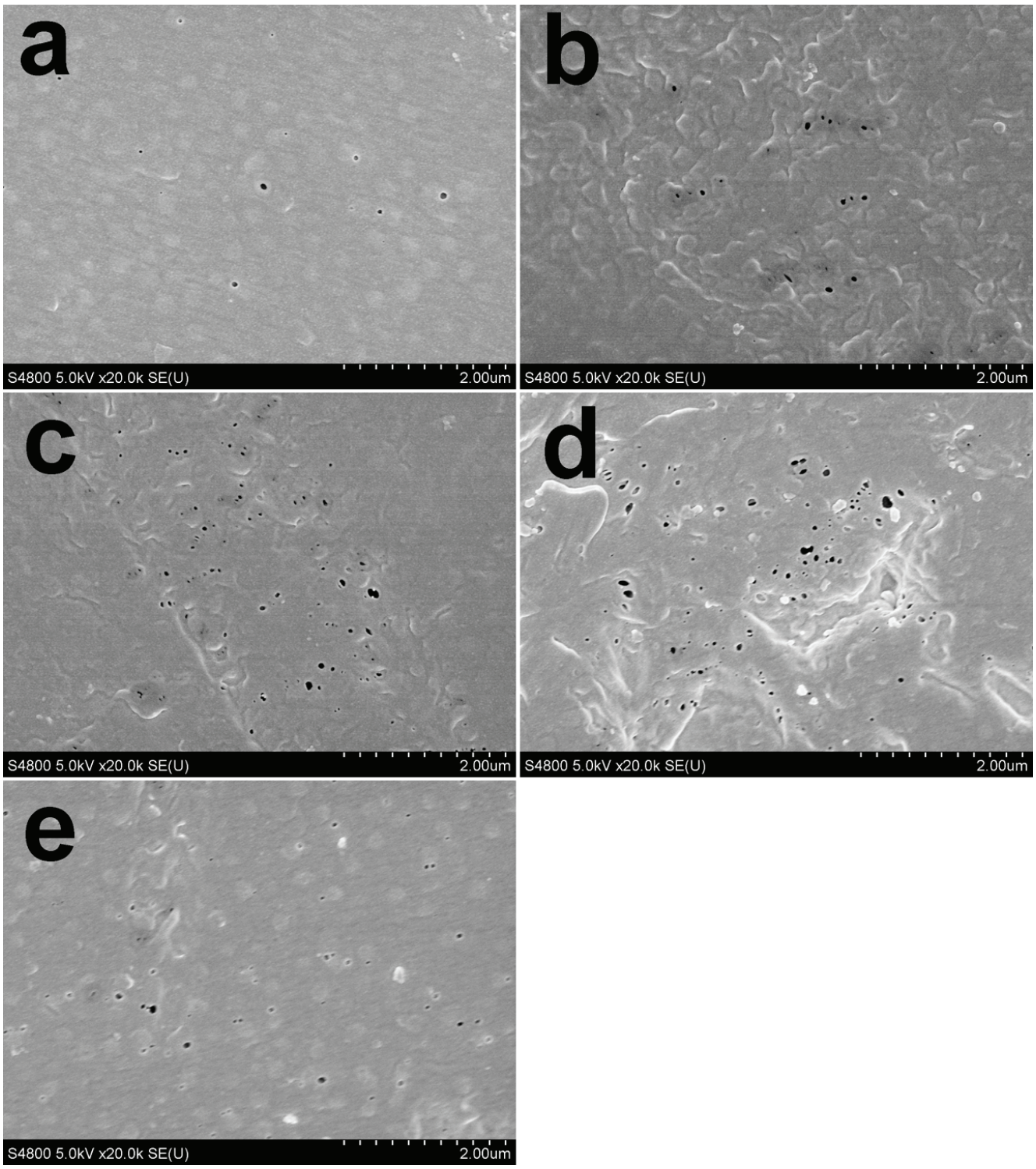

Fig. S2. Surface morphology of the membranes: (a) PVDF, (b) PVDF/MWNT$_{HPAE}$-0.5, (c) PVDF/MWNT$_{HPAE}$-1, (d) PVDF/MWNT$_{HPAE}$-1.5 and (e) PVDF/MWNT$_{HPAE}$-2.

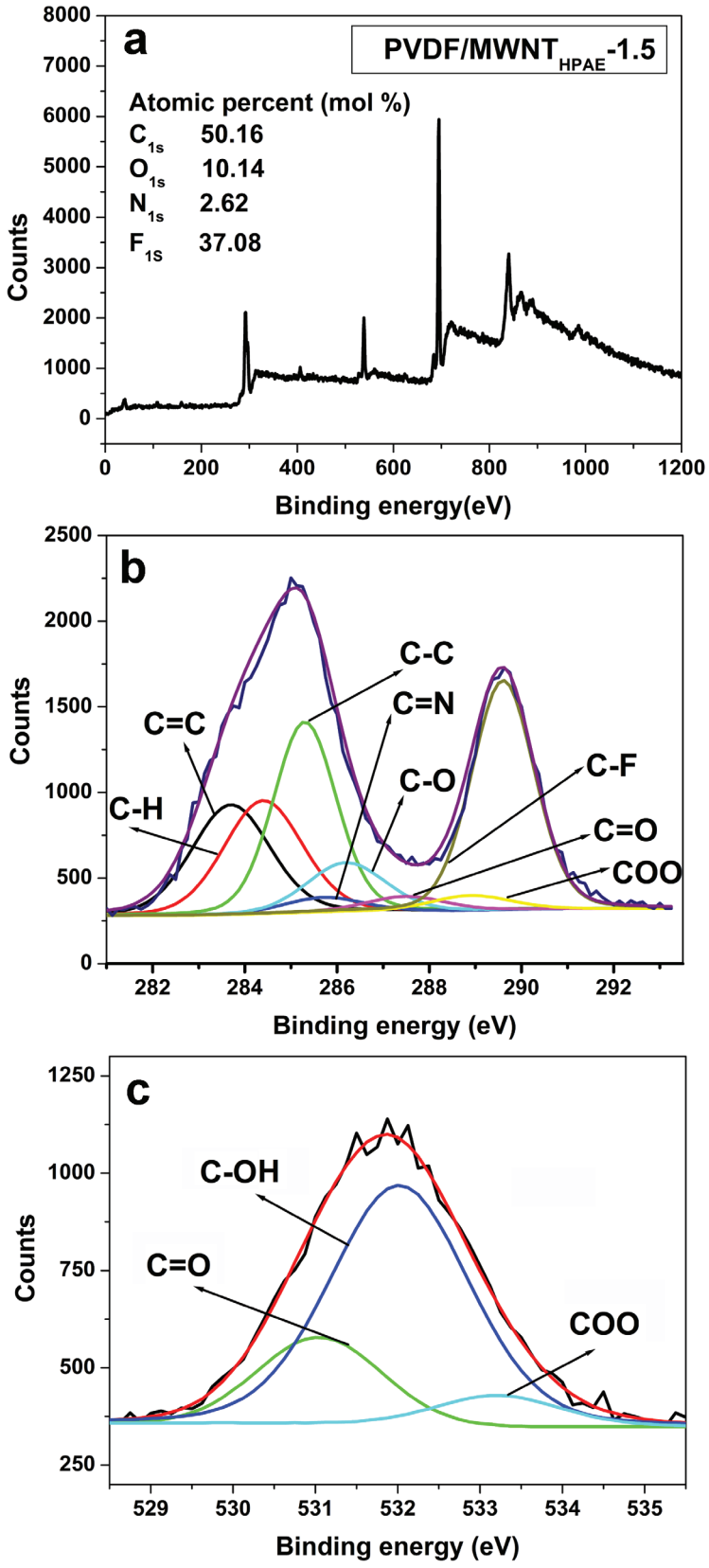

Fig. S3. XPS graphs of: (a) wide scan XPS spectra of the PVDF/MWNT$_{HPAE}$-1.5 membrane, (b) deconvolution of C$_{1s}$ core level spectra for the PVDF/MWNT$_{HPAE}$-1.5 membrane and (c) deconvolution of O$_{1s}$ core level spectra for the PVDF/MWNT$_{HPAE}$-1.5 membrane.